Tomographic imaging: potentials and limitations

J. Carlos Santamarina and Farshad Gheshlaghi

University of Waterloo, Department of Civil Engineering
Waterloo, Ontario N2L-3G1, Canada

ABSTRACT

The behavior of engineering systems is highly dependent on the distribution of material parameters. The goal of tomographic imaging is to invert boundary measurements to determine the field of a parameter. This paper reviews difficulties in tomographic imaging, summarizes inversion methods and ray tracing algorithms, and presents a comparative study of matrix-based inversion methods for simulated, laboratory, and field data. The effect of errors in ray-paths and travel times is assessed.

Keywords: tomography, seismic methods, inversion, matrix methods, information, errors, ray tracing, regularization.

1. INTRODUCTION

Tomography is the inversion of boundary measurements to determine the field of a chemical, electrical, thermal or mechanical parameter within a body. It involves the coherent manipulation and display of multiple planes or slices of a body (tomo: *gr.* to cut, slice). Tomographic methods are applied in medicine, astronomy, geophysics, geotechnical engineering, and material science among other applied fields. Engineering tomography is most often based on wave propagation data such as time, attenuation, or full time series. Both transmission data (e.g., cross-hole) and reflection data (e.g., from surface or from a single borehole) may be used in tomographic inversion.

The application of tomography in engineering faces difficulties not encountered in other fields. The purpose of this paper is to discuss some of these difficulties, and to identify adequate inversion methods and ray tracing algorithms. The discussion centers on travel time inversion.

2. TOMOGRAPHIC INVERSION METHODS

Given an object, a "projection" is the manifestation of the object on an observation plane. Operationally, projections are composed of multiple path-integrals of the field of a parameter s(x,y) measured at boundaries of the unknown region. Each measurement t in the projection is of the form,

$$t = \int_{\text{source}}^{\text{reciever}} s(x,y) \cdot dl \qquad (1)$$

The goal of tomography is to reconstruct the object by inverting its projections, i.e., "back-projecting" boundary measurements onto the unknown space. Measurements can be often be cast in this form (consider for example, the inversion of observed surface deflections to infer the internal field of strain). Inversion algorithms can be classified as: matrix inversion methods, iterative methods, transform methods, and other methods (e.g., uncertainty-likelihood, parametric, etc.)[1,2].

Matrix inversion methods work with a discretized space, and assume ray-propagation to invert projections. In general, these equations can be written in matrix form as,

$$\mathbf{t}=\mathbf{L}.\mathbf{s} \qquad (2)$$

where **t** is the [n,1] vector of measured travel times, **L** is the [n,m] matrix of estimated travel lengths, and **s** is the [m,1] vector of unknown pixel slowness. The aim of inversion is to solve Equation 2 to determine **s**. The matrix **L** is generally large, sparse, mixed determined, and inconsistent due to data and model errors. Table 1 summarizes the most common matrix inversion methods[1,2,3].

0-8194-1810-2/95/$6.00

Table 1: Matrix Inversion Methods

Problem definition:

- Given: a space discretized in m-pixels, n-integral measurements obtained at boundaries **t**[n,1], and the matrix **L**[n,m] that characterizes how measurements scanned the space. The rank of L is r≤min(m,n).
- Then: determine the distribution of the field parameter **s**[m,1], such that **Ls≈t**

Goal - Case	Objective Function	Inversion Equation
Even-determined: r=m=n	$L \cdot s = t$	$s = L^{-1} \cdot t$
Over-determined: n>m least square solution	min{E} where $E = (t - L \cdot s_{est})^T (t - L \cdot s_{est})$	$s_{est} = (L^T \cdot L)^{-1} L^T \cdot t$
Under-determined: r≤n<m minimum distance solution	min{D} such that L·s-t=0 where $D=(s-s_o)^T(s-s_o)$ and s_o is an initial estimate of s	$s_{est} = L^T (L \cdot L^T)^{-1} \cdot t$ or, $s_{est} = s_o + L^T (L \cdot L^T)^{-1} \cdot (t - L s_o)$
Mixed-determined: damped least squares	$\min\{E + \eta \cdot D\}$ where η is a constant	$s_{est} = (L^T \cdot L + \eta^2 I)^{-1} L^T \cdot t$
Mixed-determined: singular value decomposition	$L = U \cdot S \cdot V^T$ where U_i is eigenvector i of LL^T, V_i is eigenvector i of L^TL and the diagonal of Σ are the square root of eigenvalues i (other entries=0)	$s_{est} = V \cdot \Sigma^{-1} \cdot U^T \cdot t$
Noise in the data: regularization	$\min\{E + \lambda \cdot \lvert R \cdot s \rvert^2\}$ where λ is a constant and R is a regularization matrix	$s_{est} = (L^TL + \lambda R^T R)^{-1} L^T t$

Note:			
	Prediction error	$E = (t - L \cdot s_{est})^T (t - L \cdot s_{est})$	
	Solution length	$D=s^Ts$	
	All solutions are of the form	$s_{est}=M.t$	
	Forward simulation	$t_{pred}=L.s_{est}$	
	Replacing	$t_{pred}=L.M.t_{meas}$ and	$s_{est}=M.L.s_{real}$
	Data resolution matrix	$P_t=L.M$	ideal P_t=Identity
	Model resolution matrix	$P_s=ML$	ideal P_s=Identity

Comments:

The matrix L is called the data kernel
If r<m and E=0 the problem is "purely underdetermined"
The narrower the band of P_s and P_t, the better the prediction
All equations can be generalized for initial guess s_o (see underdetermined case)

Iterative algorithms have been most frequently used in engineering tomography. They are efficient from the point of view of information processing and storage, they are flexible and can accommodate solution-dependent modifications (e.g., ray re-tracing), and they can be used regardless of the level of determination (the solution to which they converge will depend on the degree of determination). These algorithms gradually correct the error e_i between the measured travel time t_i and the estimated travel time for each ray i, i.e., the error e_i is distributed or *backprojected* among the pixels touched by ray i in proportion to the length traveled by ray i in pixel j. Mathematically, this correction represents subsequent projections of the progressing solution onto the hyperplane of a new ray equation - Kaczmarz solution of simultaneous equations. In this form, iterative algorithms converge to the least square solution in over-determined cases, and to the minimum distance solution in underdetermined problems. ART and SIRT algorithms are based on this analysis. ART updates the vector of slowness after each ray. In SIRT, the correction of the pixel value is delayed until all rays are considered, then an average correction is applied, and a new iteration is started.

Data error prevents standard iterative algorithms such as ART and SIRT from converging to a unique solution. The image displayed on the screen fluctuates around a more or less defined solution. In problems with significant noise the error between projections and measured boundary values may not be strictly convex. In this case, error driven solutions may be trapped in local minima. Damping and regularization can be enforced on iterative solutions in parallel to the corresponding matrix solutions discussed in the previous section.

In transform methods, projections in the x-y space are 1D-Fourier-transformed and used to construct the 2D-Fourier transform of the image, **InvIm**, in the wave number space (kx,ky). Finally, the 2D-inverse Fourier transform of **InvIm** yields the desired tomographic image. Fourier Theorems prescribe how to assemble transformed projections in the 2D-Fourier space (kx,ky space). The Fourier Slice Theorem applies to the simplest case of straight projections. However, the Fourier Diffraction theorem is used when diffraction prevails (Rytov or Born approximations)[4].

Other reconstruction algorithms may be employed, taking into consideration engineering conditions and needs. For example, prior information and uncertainty (e.g., Bayesian updating, maximum likelihood), inversion based on a limited number of projections, and the explicit search for anomalies can be specifically addressed.

3. DIFFICULTIES IN TOMOGRAPHY

Imaging difficulties arise from on-site implementation, the physics of seismic wave propagation, and mathematical issues in inversion. Salient adversities and pitfalls in each category are discussed in this section.

3.1. Testing Difficulties

This set of problems includes source restrictions (directivity of different propagation modes, amplitude, repeatability), triggering errors (difficulties in stacking), noise (ambient, mechanical, electromagnetic, filtering and phase shift), source and receiver coupling to object, detection of true first arrivals, and accessibility to different faces of the object. The latter will reflect on uneven distribution of information content, which is further discussed later in the sequel.

3.2 Physical Limitations

Heterogeneity. Heterogeneity modifies spherical wave fronts, elongating them in the direction of higher velocity. When rays are drawn (normal to wave fronts), ray bending is observed.

Anisotropy. Wave propagation in anisotropic media is complex: energy in shear waves splits, the ray direction is given by the direction of energy transport, the ray is not perpendicular to the wave front ("quasi" P or S waves), and the ray direction does not necessarily remain in the plane. Anisotropy alone does not lead to curved ray paths; however, anisotropy couples with vertical heterogeneity to deviate rays from the simplest straight-path condition.

Reflection and Refraction. At the interface between two materials with different impedance $I=\rho.v$ (ρ: material density; v: velocity), part of the energy is transmitted and part of the energy is reflected. Furthermore, mode conversion takes place: incident P-waves are reflected and refracted as P and S-waves; the same occurs with the S-wave component normal to the interface. Generalized Snell's laws characterize the effect of interfaces.

Ray Assumption. The interaction of waves with inclusions depends primarily on the size of the inclusion D with respect to the wave length λ. The ray assumption applies when $D>>\lambda$. More specifically, ray tomography is applicable when the scale length of the anomaly is at least the radius of the first Fresnel zone: if the average ray length is n wavelengths, the size of the inclusion must be at least $\xi\cdot\lambda\cdot(n)^{0.5}$, where ξ varies between 0.5 and 1. The "straight ray" assumption dominated the development of engineering tomography during the 80's, as an extension of X-ray tomographic imaging in medical applications. From optics, the straight ray approximation applies if the travel length $L>>\lambda/2\pi$, if the wavelength is significantly smaller than the size of the anomaly, and if velocity changes are less than 20% to 30%.

Diffraction. When the size of inclusions is within the same order of magnitude as the wavelength, the ray approximation does not hold, and propagation must be considered from the point of view of the wave front and scattered energy. Diffraction degrades the quality of tomograms when the linear ray assumption is made: low velocity inclusions are imaged smaller than real size,

while high velocity anomalies are imaged larger. Low velocity anomalies are more sensitive to diffraction than high velocity ones, and their detection becomes difficult when the plane of receivers is located about twice the diameter of the inclusion away from it.

Fresnel's ellipse. The position of scatterers that affect wave arrival at the source is related to the wave length λ. Indeed, waves scattered from diffractors within an ellipse, so that the travel distance is the straight distance d plus $\lambda/4$ or $\lambda/2$, will arrive in phase with the direct wave travelling the straight path d. This observation is relevant in selecting ray-tracing algorithms (often a "thick ray" assumption is used), and in selecting source and receiver configuration: transducers too close together do not necessarily add information content.

3.3 Mathematical Problems

Size and sparsity. The matrix **L** is sparse. Storage and computation time can be decreased more than one order of magnitude when adequate computational techniques are used. In a dense N×N matrix, the order of computation complexity is $O(N^3)$ and $O(N^2)$ for storage. The application of direct methods with sparse matrix techniques requires $O(N^2)$ and $O(N^{\sim 1.4})$, respectively. However, efficient iterative algorithms combined with sparse matrix techniques can reduce the order of computational complexity to $O(N^{1.3})$ and storage requirement to O(N).

Ray bending and non-linearity. If ray bending takes place, ray paths depend on inverted pixel velocities, thus the tomographic problem becomes non-linear. If it is appropriate to consider propagation in terms of rays, ray bending can be taken into consideration in iterative algorithms and matrix methods. In this non-linear problem, ray paths depend on the velocity field. Thus, the matrix of travel lengths L_{ij} is not constant and must be recalculated with a digital ray-tracing algorithm as the field of velocity evolves during successive iterations or inversions. Ray tracing algorithms assume Fermat's "shortest time" criterion, and they are categorized as: one-point methods, two-point methods, and whole field methods. Table 2 presents a summary of ray tracing approaches, their advantages and limitations[5,6,7,8].

Table 2: Ray Tracing Methods

Method	Procedure	Abilities	Short comings
One Point Methods	1. Generate initial guess for take-off angle. 2. Trace rays from source to receiver (Snell's Laws). 3. Repeat till minimum time.	• Suitable for 3D ray tracing. • Useful for cases with unknown source location. • Easy to apply. • Limited computer memory.	• Not for diffracted rays and ray paths in shadow zones. • Not always converge. • Unable to handle head waves.
Two Point Methods	1. Assume an initial ray path. 2. Perturb the path and compute travel time. 3. Repeat till minimum time.	• Always converge to a solution. • Can find diffracted rays and rays in shadow zones.	• Solution may converge to local minima. • Demand more computer memory than one-point methods.
Whole Field Methods	1. Generate all cell segments. 2. Compute travel time for different segments. 3. Find best path (graph search).	• Compute diffracted ray paths, and paths in shadows. • Avoid numerical instabilities wherever velocity changes abruptly.	• Significant computation time and memory demand. • Angle of refraction may not change continuously with angle of incidence.

Uneven Distribution of Information. The distribution of information content is primarily dependent on the location of sources and receivers. It is also affected by the field of velocity, in as much as it modifies the ray paths. Figure 1 shows the density of rays in pixels for cross-board testing, for three different velocity fields: (a) homogeneous, straight path, (b) central high velocity inclusion, $v_{inc}=1.2\ v_{back}$, and (c) central low velocity inclusion, $v_{inc}=0.8\ v_{back}$. Underdetermined and overdetermined regions are clearly insinuated. Uneven distribution of information magnifies the difficulties in inversion in the presence of data or model errors, and noise appears in the form of ghosts, "dumped" in low information regions.

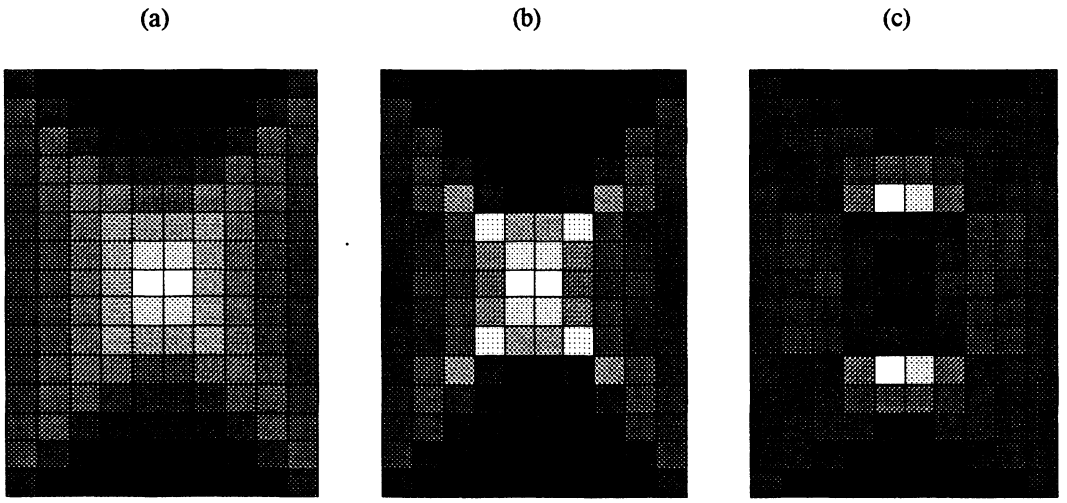

Fig. 1. Distribution of information in cross-board illumination. (a) homogeneous velocity field - straight rays, (b) high velocity anomaly - curved rays, and (c) low velocity anomaly - curved rays. Dark indicates low information content.

Underdetermined problems. A large number of measurements does not necessarily imply an over-determined condition. Many measurements may eventually provide the same information, effectively reducing the number of independent observations (in cross-board data, less than half the measurements are truly independent). When the problem is underdetermined, there are infinite number of solutions that result in null prediction error (purely underdetermined). Two alternatives are either to add "a priory information" (e.g., values are non-negative, media is layered, velocity field is smooth), or to reduce the problem size (fewer pixels, or set problem in parametric terms). A common choice is to identify the solution of minimum norm, $\min(\mathbf{s}^T\mathbf{s})$. If an initial guess of **s** is available, $\mathbf{s}_o$, the minimum norm solution becomes the minimum distance solution

Overdetermined Problems. In practice, a wave from a source is detected by multiple receivers, creating a "fan" of rays out of each source. If the number of measured, independent travel times n exceeds the number of pixels m, n>m, the problem is over-determined, and tomographic reconstruction attempts to find the best estimate of **s**. The error e_i between a measured travel time t_i and the estimated travel time for each ray i is $e_i=(\mathbf{t}-\mathbf{L}\mathbf{s})_i$. Several measures of error, called *norms*, could be minimized; for example, $\min(\Sigma|e_i|)$, $\min(\Sigma(e_i)^2)$, or $\min(\max(e_i))$. The second alternative is the least squares solution.

Mixed-determined Problem. Given the uneven distribution of information content in engineering problems, there will be over-determined and underdetermined regions within the image. The first, semi-intuitive alternative is to look for a solution that combines minimum norm and minimum error; this is the damped least squares solution. A more elaborate approach is obtained based on the singular value decomposition of matrix L.

Data and Model Errors. It is possible to add information by enforcing properties to the solution. For example, one could require global smoothness (minimum second derivative) or just horizontal smoothness if layered media is expected. This is done by adding the chosen additional constraint to the objective function. This "trick" is called regularization. The regularization matrix may be the smoothing operator, or some physical constraint. The model selected for wave propagation may add additional errors which affect the values estimated in **L** (model errors). The solution for this case is called total least squares[3].

4. TOMOGRAPHIC STUDIES

Several studies are presented in this section. Simulated data, measurements conducted in the laboratory and field data are analyzed. Cases are sketched in Figure 2. Only cross-board data is considered in all cases, to assess a typical field situation with limited illumination angles. All inversions are conducted with matrix solutions, implemented with efficient iterative algorithms for sparse matrix computations. Both straight and curved rays are used. The selected two point ray tracing algorithm involves sine-arcs which are used to perturb the straight path; the amplitude of the arc is optimized until the travel time is minimum.

(a) Simulated cases: low and high velocity anomalies at center and off-center (HV-Cent, LV-Cent, HV-Off, LV-Off)

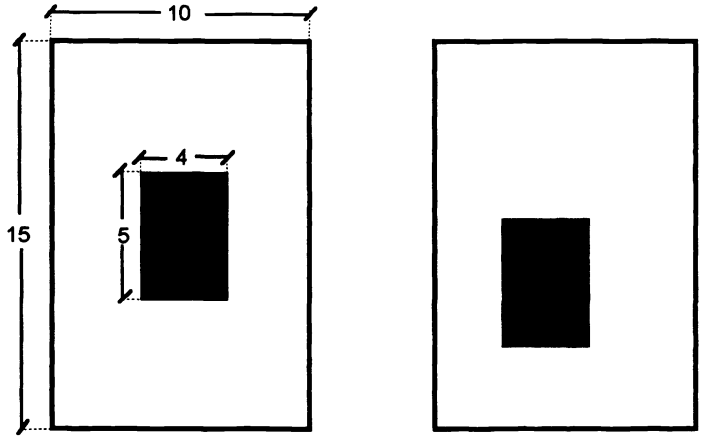

(b) Laboratory study with acoustic tomographer - high velocity anomalies

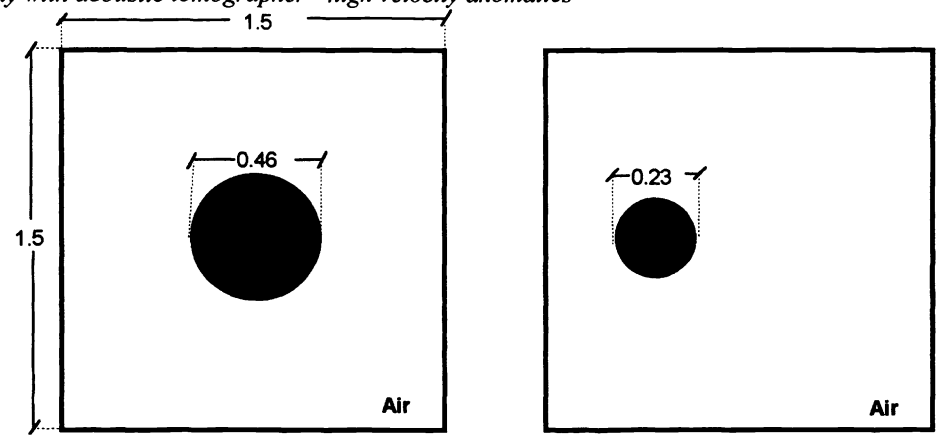

(c) Field study: concrete column

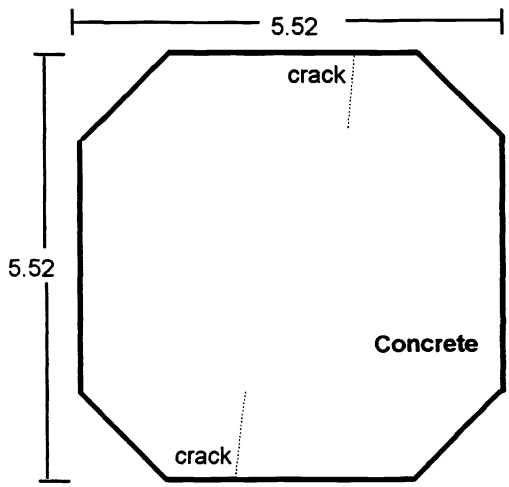

Fig. 2. Simulated cases, laboratory study of high velocity anomalies and field testing of concrete column.

4.1 Damped Least Squares Solution: Optimal Damping

The simulated cases (Figure 2-a) were investigated to determine the optimal damping coefficient η. Straight paths were used. Therefore, the matrix **L** is the same in all cases. Results are presented in Figure 3, in terms of the average absolute error (AAE) in pixel velocity between the input image and the inverted output image (normalized with respect to the average pixel velocity):

$$AAE\% = \frac{\sum_{pixels} \left| V_j^{real} - V_j^{inv} \right|}{m} \frac{1}{V_{ave}} * 100 \qquad (3)$$

It can be seen that the quality of the image worsens with either lacking or excessive damping, and that optimal damping depends on the velocity field.

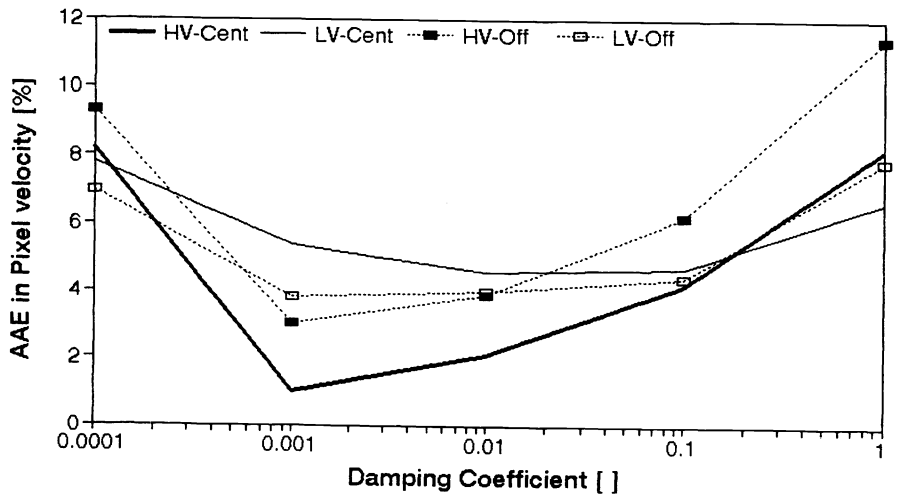

Fig. 3. Damping coefficient and image quality. Four simulated cases

4.2 Measurement Error, Model Error and Inversion Error (Damped Least Squares)

Significant deviations in ray path can often imply only minor differences in travel time (e.g., compare the time along a straight path between two points with respect to the time along a bi-linear path). Thus, one must question the accuracy needed in ray tracing algorithms, not for time prediction, but for the computation of pixel travel lengths in **L**. In order to study this effect, the simulated cases described in Figure 2-a were considered. The test method follows: (1) the vector of travel times $\mathbf{t}_{opt}$ and the matrix of lengths $\mathbf{L}_{opt}$ are determined for optimal travel paths (wide scanning with small step), (2) alternative paths are selected by restricting the scanning step in the ray tracing algorithm and corresponding times are computed, **L'** and **t'**, (3) the image is inverted in each case, using a constant damping coefficient η=0.005, and the velocity vector is obtained for the optimal case and other cases, $\mathbf{V}_{opt}$ and **V'**, (4) error in path, time and velocity are computed.

Two error norms were used, sum of absolute values (Equation 3) and sum of square values, producing similar trends. Figure 4-a shows that the average absolute error AAE in pixel travel time computed with rays of different curvature is related to the AAE in travel length per pixel. However, only a 1% error in time relates to an average 4-pixel widths difference in travel length per pixel (400%); given that the average travel length per pixel is 20 pixel widths, the percent average error is 4/20=20%. Figures 4-b-&-c show that the error in pixel velocities can be justified as a result of error in measurement or error in ray paths, i.e., ray model. It can be concluded that while more accurate travel paths can improve the inverted image, the demand on accurate ray paths must not exceed measurement accuracy on travel times, which is usually about 1%. High velocity central anomalies can be best resolved with cross-hole data; accuracy decreases for low velocity anomalies and off-center anomalies. These observations corroborate the trends observed in the distribution of information content (Figure 1). Higher local errors in inverted velocities above and bellow high velocity zones are due to the low information content in these areas resulting from ray deviation towards the anomaly (Figure 1b).

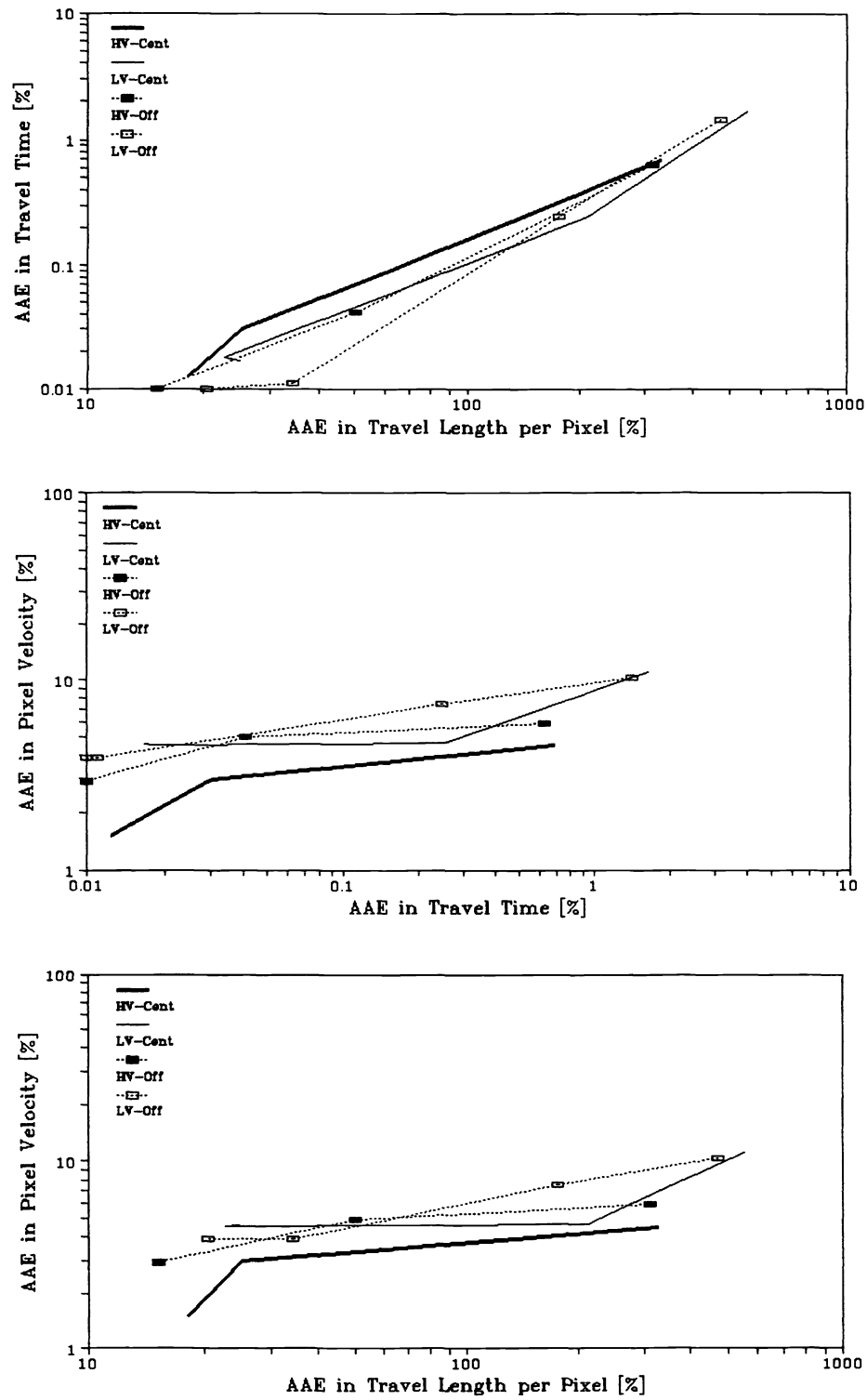

Fig. 4. Image quality versus the accuracy in travel time measurements and ray tracing.

4.3 Damped Least Squares vs Regularization

Simulated data obtained with straight-rays for the case presented in Figure 2-a (high velocity central anomaly) were inverted using damped least squares and regularization. Damping and regularization coefficients η and λ were gradually changed until optimal images were obtained. The best images are shown in Figure 5, and they indicate that regularization is also an effective alternative to lessen the problems of mix-determination.

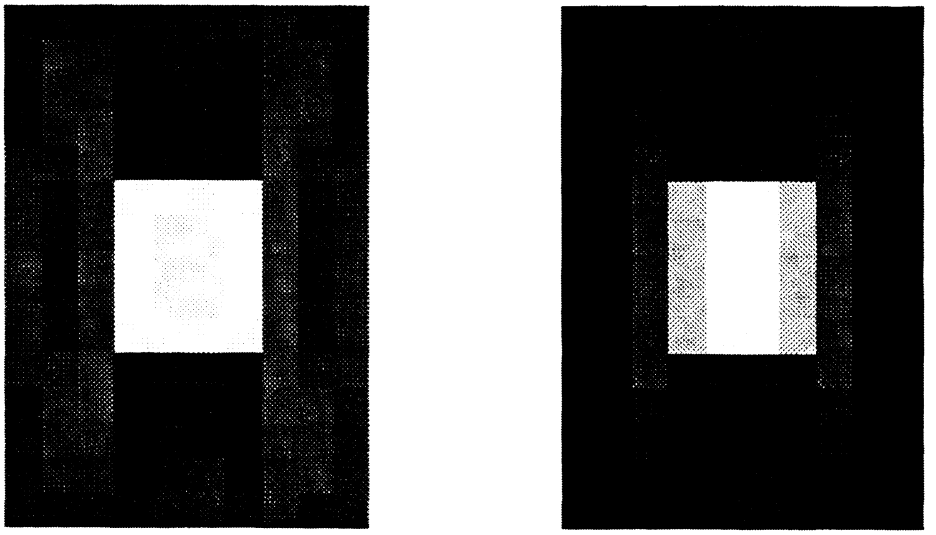

Fig. 5. Inversion study with simulated data for high velocity anomaly at the center. (a) Damped least squares, (b) Regularization.

4.4 Regularization: Laboratory data

An acoustic tomographer was built to determine cross-board travel time data in the laboratory. The background medium is air. Selected anomalies are placed within the instrumented frame. Micro-explosives, microphones and a multi-channel digital storage oscilloscope complete the setup.

A high velocity anomaly was simulated by placing a helium balloon at the center of the frame. Times were measured between 16 sources and 16 receivers, and inverted with different values of the regularization coefficient λ, using straight rays. The resulting pixel values were used to re-trace rays for a second iteration with bent rays. The second inversion for each set was repeated with the same regularization coefficient. The coefficient of variation for pixel values in each image is plotted in Figure 6-a (CoV is the ratio of the standard deviation and the mean of pixel values). The figure shows three regions: high variability for low λ, very low variability for high λ (the velocity field becomes uniform for excessive smoothing), and an intermediate region with acceptable inversions for a relatively wide range in regularization coefficient λ. Inversions with curved rays lead to higher variability because they tend to preserve the contrast in the region. However, the trend of CoV-vs-λ is very similar in both cases. Thus, optimal regularization coefficients can be selected with straight rays.

The average square error ASE in pixel velocity between inverted images and the known real pixel velocities are plotted versus the regularization coefficient λ in Figure 6-b, where

$$ASE\% = \sqrt{\frac{\sum_{pixels}\left(V_j^{real} - V_j^{inv}\right)^2}{m}} * \frac{1}{V_{ave}} * 100 \qquad (4)$$

The increase in regularization diminishes the effect of high pixel variability and the square error ASE. However, excessive regularization flattens pixel values within the anomaly increasing the deviation of the image from the true condition. Curved

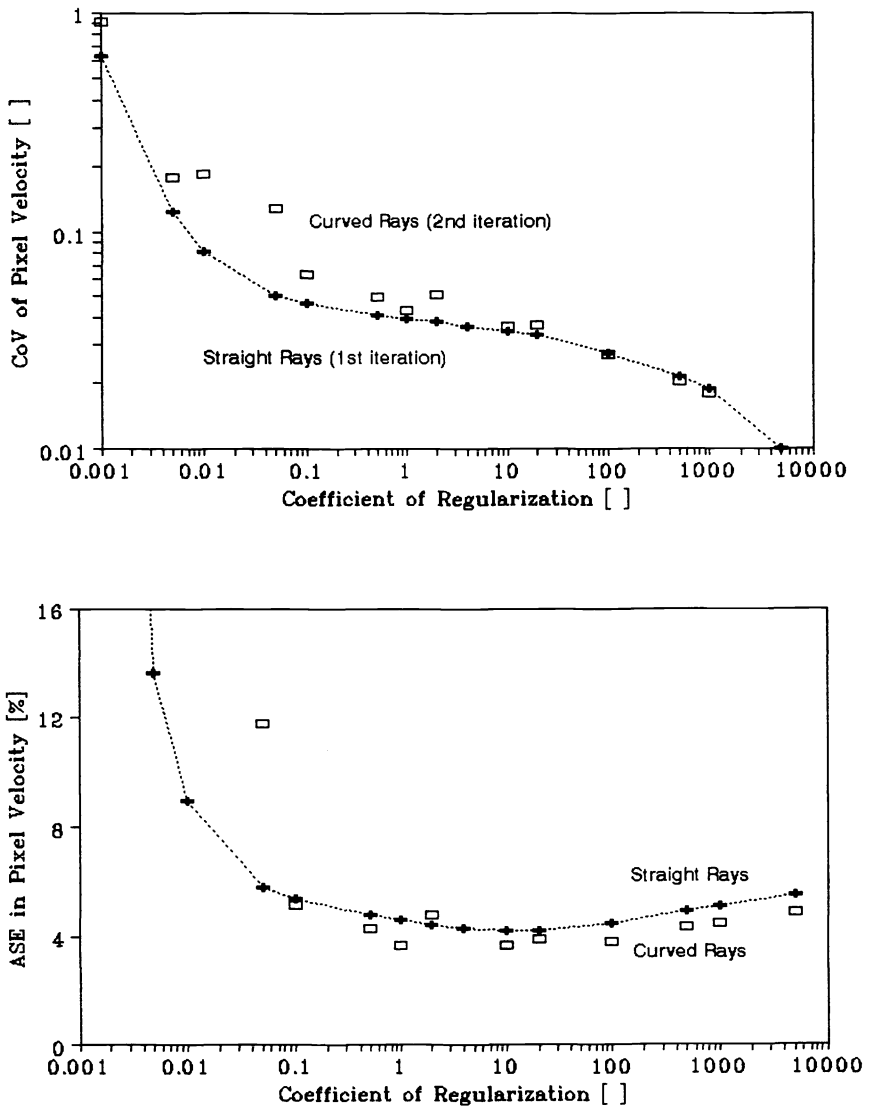

Fig. 6. Inversion of laboratory data: The effect of the coefficient of regularization λ. (a) Variability. (b) Resolvability

rays magnify the effect of variability at low λ, however, they lead to better images for all values of λ above a threshold of smoothness. These plots highlight the underlying trade-off between resolution and variance[1]. A similar study was conducted with a smaller high velocity anomaly placed off-center, and tested with 7 sources and 7 receivers (very limited information). Results are identical to those shown in Figures 6-a&b. Tomograms for these two cases are shown in Figure 7.

4.5 Concrete Column (very noisy data)

A pier of the Kosciuzko bridge, New York, was tested using an impact source and piezocrystals (Figure 2-c). The pier showed a transverse "closed" crack, all along the height of the pier, which appeared to be continuous between two parallel faces. Ambient mechanical noise, traffic induced vibrations, and electromagnetic noise were significant. Two cross-board data sets were obtained. Inversions were conducted for different regularization coefficients. Final conditions were selected following the criteria discussed above. Results are presented in Figure 8. The crack is apparent only for measurements conducted in the parallel direction. Physical and mathematical reasons support this observation (i.e., travel time delays are minimal for normal shooting, and the problem is non-unique).

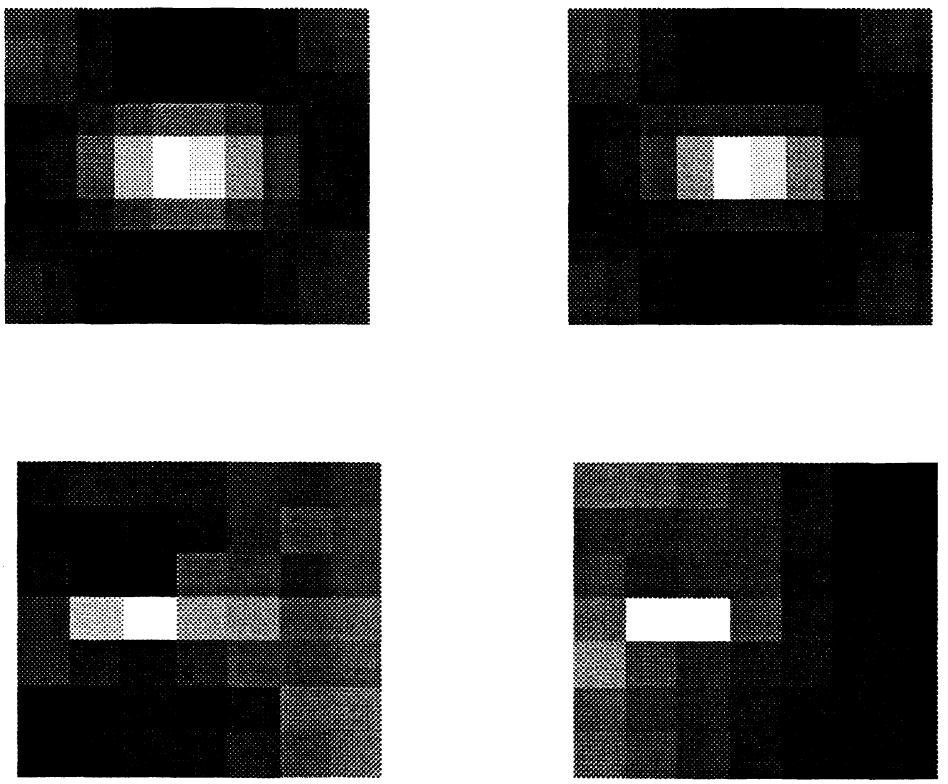

Fig. 7. Inversion of laboratory data with regularization: straight (left) and curved (right) rays. (a) Central, high velocity anomaly, 256 rays, λ=10. (b) Off-center high velocity anomaly, 49 rays, λ=1 (Refer to Figure 2-b).

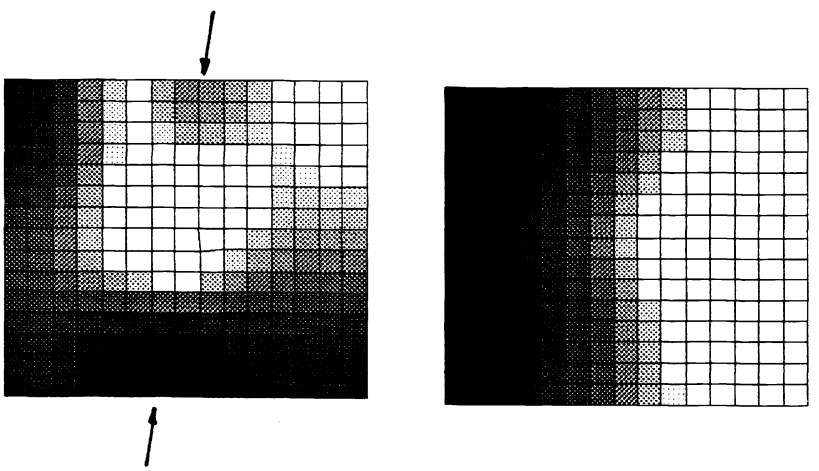

Fig. 8. Inversion of field data with regularization: concrete column. (a) cross-board data parallel to crack, 225 rays (b) cross-board data normal to crack, 225 rays (Refer to Figure 2-c).

5. CONCLUSIONS

A high percentage of cross-board measurements are linearly dependent, therefore, the real level of information content is lower than predicted by the number of measurements. In general, limited illumination angles lead to underdetermined and mix-determined problems. In the case of underdetermined problems, multiple solutions are possible which produce travel times identical to measured times. In this case, convergence-control by minimization of time error is irrelevant.

The distribution of information content is primarily dependent on the location of sources and receivers, yet, it is also influenced by the field of velocity. The resolvability of an anomaly is affected by shot-direction, and may be restricted by "diffraction healing" of the wave front.

Studies with simulated cross hole data for typical engineering applications show that only a 1% error in time relates to an average 20% error in travel length per pixel. Hence, accuracy in ray tracers may be relaxed. It can be concluded that while more accurate travel paths can improve the inverted image, the demand on accurate ray paths must not exceed measurement accuracy on travel times.

Inversions can be conducted with different regularization coefficients λ, however, there is a trade-off between resolution and variance. A plot of the coefficient of variation for each image versus the value of λ can be used to select optimal regularization coefficient within the transition region between high noise and over-smoothed image. This region is common to straight and curved rays. Hence, an estimate of λ_{opt} can be identified with straight rays, before iterations with curved rays are conducted. Curved rays should be used for $\lambda \approx \lambda_{opt}$; in this range, curved rays will enhance contrast without decreasing the quality of the image.

6. ACKNOWLEDGMENTS

This research is part of a project on Wave-Material Interaction and Applications. T. Wakim and A. Tallin participated in the testing of the column. Support was provided by the Natural Sciences and Engineering Research Council of Canada.

7. REFERENCES

1. W. Menke, Geophysical Data Analysis: Discrete Inverse Theory, Academic Press, New York, 1989.
2. J. C. Santamarina, "An introduction to Geotomography," Geophysical Characterization of Sites, Edited R. D. Woods, Int. Science, New Hampshire, 1994.
3. G. H. Golub and C. F. Van Loan, Matrix Computations, John Hopkins U. Press, Baltimore, MD, 1989.
4. A. C. Kak and M. Slaney, Principles of Computerized Tomographic Imaging, IEEE Press, New York, 1988.
5. F. Gheshlaghi and J. C. Santamarina, "Ray tracing algorithms," Dept. Civil Engineering, University of Waterloo, 1994.
6. T. J. Moser, "Shortest path calculation of seismic rays," Geophysics, Vol. 56, No. 1, pp. 59-67, 1991.
7. R. J. Lytle and K. A. Dines, "Iterative ray tracing between boreholes for underground image reconstruction," *IEEE Trans. Geosc. Remote Sens.*, vol. 18, pp. 234-240, 1980.
8. C. H. Thurber and W. L. Ellsworth, "Rapid solution of ray tracing problems in heterogeneous media," Bulletin of the Seismological Society of America, Vol. 70, No. 4, pp. 1137-1148, 1980.